Probing the essential catalytic residues and substrate affinity in the thermoactive Bacillus stearothermophilus US100 L-arabinose isomerase by site-directed mutagenesis.

M. Rhimi, M. Juy, N. Aghajari, R. Haser, S. Bejar

JOURNAL OF BACTERIOLOGY, May 2007, p. 3556–3563 Vol. 189, No. 9
0021-9193/07/$08.00+0 doi:10.1128/JB.01826-06

Probing the Essential Catalytic Residues and Substrate Affinity in the Thermoactive *Bacillus stearothermophilus* US100 L-Arabinose Isomerase by Site-Directed Mutagenesis▽

Moez Rhimi,[1] Michel Juy,[2] Nushin Aghajari,[2] Richard Haser,[2] and Samir Bejar[1]*

Laboratoire d'Enzymes et de Métabolites des Procaryotes, Centre de Biotechnologie de Sfax BP "K," 3038 Sfax, Tunisie,[1] and Laboratoire de BioCristallographie, Institut de Biologie et Chimie des Protéines, UMR 5086-CNRS/Université de Lyon 1, IFR128 "BioSciences Lyon-Gerland," 7 Passage du Vercors, F-69367 Lyon Cedex 07, France[2]

Received 5 December 2006/Accepted 19 February 2007

The L-arabinose isomerase (L-AI) from *Bacillus stearothermophilus* US100 is characterized by its high thermoactivity and catalytic efficiency. Furthermore, as opposed to the majority of L-arabinose isomerases, this enzyme requires metallic ions for its thermostability rather than for its activity. These features make US100 L-AI attractive as a template for industrial use. Based on previously solved crystal structures and sequence alignments, we identified amino acids that are putatively important for the US100 L-AI isomerization reaction. Among these, E306, E331, H348, and H447, which correspond to the suggested essential catalytic amino acids of the L-fucose isomerase and the L-arabinose isomerase from *Escherichia coli*, are presumed to be the active-site residues of US100 L-AI. Site-directed mutagenesis confirmed that the mutation of these residues resulted in totally inactive proteins, thus demonstrating their critical role in the enzyme activity. A homology model of US100 L-AI was constructed, and its analysis highlighted another set of residues which may be crucial for the recognition and processing of substrates; hence, these residues were subjected to mutagenesis studies. The replacement of the D308, F329, E351, and H446 amino acids with alanine seriously affected the enzyme activities, and suggestions about the roles of these residues in the catalytic mechanism are given. The mutation F279Q strongly increased the enzyme's affinity for L-fucose and decreased the affinity for L-arabinose compared to that of the wild-type enzyme, showing the implication of this amino acid in substrate recognition.

L-Arabinose isomerases (L-AIs; EC 5.3.1.4) catalyze the conversion of L-arabinose to L-ribulose in biological systems. They are also referred to as D-galactose isomerases due to their ability, in vitro, to isomerize D-galactose into D-tagatose (4). The latter sugar is of importance when one considers the privileged position of this isomer of D-galactose in sweeteners. D-Tagatose is a rare natural ketohexose having a taste and physical properties similar to those of sucrose (24). Additionally, D-tagatose is an antihyperglycemic factor, an efficient antibiofilm with a very low-calorie carbohydrate, and a bulking agent (20, 36). It has been the subject of recent interest in the food and drug industry and is considered to be a safe and low-calorie substance in the United States (17).

The majority of L-AIs previously described, such as those from *Escherichia coli* and *Mycobacterium* and *Lactobacillus* species, are not thermoactive (9, 35). Isomerization at high temperatures increases the reaction rate and allows a shift in the equilibrium between D-galactose and D-tagatose towards the latter, which is desirable for industrial use (12). For this reason, many thermoactive and thermostable L-AIs have been isolated and studied, including those derived from members of the genera *Thermotoga*, *Geobacillus*, *Thermoanaerobacter*, and *Thermus* (10, 14, 17, 18).

In their functional conformations, the L-AIs have been shown to adopt a hexameric quaternary structure, as observed in the thermolabile L-AI from *E. coli*, or a tetrameric quaternary structure, as found in the L-AIs from *Thermotoga* and *Geobacillus* species (17, 18).

Genetic engineering of several L-arabinose isomerases has been performed using the error-prone PCR procedure in order to improve their suitability for biotechnological applications. Kim et al. have successfully increased the optimal temperature of *E. coli* L-AI from 30 to 60°C by introducing the concomitant H228D, G384D, S393T, K428N, and D475K mutations (15). Furthermore, these mutations improved the catalytic properties of the *E. coli* L-AI and shifted the bioconversion rate to 50%, compared to 20 to 30% for the wild-type enzyme (15). Recently, Kim et al. reported that the mutations M322V, S393T, and V408A in an L-AI mutant derived from *Geobacillus stearothermophilus* increased the D-galactose isomerization activity, the optimum temperature, the catalytic efficiency for D-galactose, and the rate of production of D-tagatose from D-galactose (13).

Nevertheless, the majority of L-AIs have high optimum pHs, which is a major drawback for industrial applications, since isomerization at high temperatures and under alkaline conditions leads to unwanted side reactions generating undesirable subproducts (19). Recently, the key role of K269 in the acidotolerance of *Alicyclobacillus acidocaldarius* L-AI was reported (19). A mutation introduced at the equivalent position (D268K) in *Bacillus halodurans* L-AI decreased the optimum pH of the enzyme from 8.0 to 7.0 (19).

While all previously reported mutations play an important role in the improvement of the enzymatic properties, no struc-

* Corresponding author. Mailing address: Laboratoire d'Enzymes et de Métabolites des Procaryotes, Centre de Biotechnologie de Sfax BP "K," 3038 Sfax, Tunisie. Phone: 216 74 44 04 51. Fax: 216 74 44 04 51. E-mail: Samir.bejar@cbs.rnrt.tn.

▽ Published ahead of print on 2 March 2007.

tural explanation was provided in previous studies due to the absence of a three-dimensional (3D) structure of an L-AI. Very recently, the 3D structure of *E. coli* L-AI was determined (23). However, a detailed analysis of the structure-function relationships of this isomerase was not reported. In addition, no information was given concerning the isomerization mechanism and the amino acids implicated, except for residues E306 and E333, which correspond to the catalytic residues identified in *E. coli* L-fucose isomerase (L-FI), also known as D-arabinose isomerase (31).

We have previously described the cloning, overexpression, purification, and characterization of a thermostable L-arabinose isomerase isolated from the thermophilic *Bacillus stearothermophilus* US100 strain. The purified enzyme is a homotetramer with a molecular mass of 56 kDa for each monomer (28). US100 L-AI has an optimum temperature of about 80°C and an optimum pH between 7.5 and 8.0 and differs from earlier reported L-AIs in its behavior towards metallic ions (28).

Here we report the identification of the essential catalytic amino acids implicated in the isomerization reaction of US100 L-AI by using site-directed mutagenesis and 3D structure homology modeling. In addition, the enzyme's affinity features were investigated.

MATERIALS AND METHODS

Bacterial strains, plasmids, and media. *E. coli* HB101 (F^- *hsdS20 ara-1 recA13 proA12 lacY1 galK2 rpsL20 mtl-1 xyl-5*) was used as an Ara^- mutant host strain and also for the purification of the recombinant L-AIs. The plasmid pMR5 containing the wild-type US100 *araA* gene (28) was used for the production of the wild-type US100 L-AI protein. pMR12, pMR13, pMR14, pMR15, pMR16, pMR17, pMR18, pMR19, and pMR20 are the recombinant plasmids carrying the mutated US100 *araA* gene (Table 1). The culture of different *E. coli* strains harboring wild-type and mutated genes was done in Luria-Bertani medium (30) supplemented, when necessary, with ampicillin (100 μg/ml) and IPTG (isopropyl-β-D-thiogalactopyranoside; 160 μg/ml).

DNA manipulation and PCR. The preparation of plasmid DNA, digestion with restriction endonucleases, and separation of fragments by agarose gel electrophoresis were performed as described by Sambrook et al. (30). PCRs were carried out with a Gene Amp PCR System 9700 (Applied Biosystems). The amplification reaction mixtures (100 μl) contained *Pfu* (*Pfu* DNA polymerase) amplification buffer, 10 mM $(NH_4)_2SO_4$, 10 pmol of each primer, 100 ng of DNA template, and 2 U of *Pfu* enzyme (Appligene). The cycling parameters were 94°C for 5 min followed by 40 cycles at 94°C for 30 s, 55°C for 60 s, and 72°C for 120 s.

Construction of L-arabinose mutant enzymes. L-Arabinose isomerase mutant enzymes were generated using the US100 L-AI wild-type coding sequence in plasmid pMR5 as the template. Mutations were introduced by site-directed PCR mutagenesis. Thus, two nonmutagenic external primers, F-araA (5′-GTGAAC GGGGAGGAGCAATG-3′) and R-araA (5′-GAAATCTTACCGCCCCCGC C-3′), and two partial complementary internal primers containing the desired mutation were designed (Table 1).

For each mutation, two separate PCRs were done and the resulting fragments were amplified using pMR5 as the template with the corresponding primers for each reaction. The resulting two PCR fragments were extracted separately, and then a third amplification was carried out with a mixture containing these fragments in the presence of the external primers. The PCR products were purified using the GFX PCR DNA and gel band purification kit by following the instructions of the manufacturer (Amersham Biosciences).

The purified mutated DNA fragments were cloned into a pUT57 vector, previously linearized with the SmaI restriction enzyme, and the *E. coli* HB101 strain was transformed with the vector. Transformants were plated on Luria-Bertani medium supplemented with ampicillin (100 μg/ml) and IPTG (160 μg/ml). The obtained colonies were analyzed by restriction, and mutations were confirmed by DNA sequencing using an automated DNA sequencer (Applied Biosystems). Obtained mutations are listed in Table 1.

Preparation of crude extracts and protein purification. Cells were harvested by centrifugation at 7,500 × *g* for 10 min, and the pellets were suspended in 100 mM HEPES buffer supplemented with 1 mM $MnSO_4$ and 0.2 mM $CoCl_2$. Then cell suspensions were incubated for 2 h on ice in the presence of 5 mg of lysozyme/ml, 100 mM phenylmethylsulfonyl fluoride, and 2 μg of pepstatin A/ml. Cell disruption was carried out by sonication at 4°C for 6 min (pulsations of 3 s at 90 A) by using a Vibra-Cell 72405 sonicator, and cell debris was removed by centrifugation (30,000 × *g* for 30 min at 4°C).

TABLE 1. Oligonucleotides used for site-directed mutagenesis

Desired mutation	Primer sequence[a]	Plasmid
E306A	GATTTGGCGGCGCAGGCGACTGG	pMR12
D308A	CGGCGAAGGCGCCTGGAAAACGG	pMR16
F279Q	CTTTACGACGACGCAAGAAGATTTGCA	pMR20
F329A	AAAGGAACATCGGCCATGGAAGACTA	pMR18
E331A	ACATCGTTCATGGCAGACTACACG	pMR13
H348A	CTTGGCGCGGTTATGCTCGAAGTA	pMR15
E351A	GCGCATATGCTCGCAGTATGCCCGACG	pMR17
H446A	AGCCGGCGGAGCGGCTCACACATGCTT	pMR19
H447A	GGCGGAGCGCATGCCACATGCTTC	pMR14

[a] Nucleotide sequences corresponding to the mutated amino acids are underlined.

For protein purification, crude cell extract from each strain was heated (70°C for 30 min) and centrifuged at 30,000 × *g* for 30 min at 4°C. Proteins were precipitated between 50 and 80% acetone saturation, suspended in 100 mM HEPES buffer (pH 7.5), concentrated, and desalted in centrifugal microconcentrators (Amicon, Inc.) with a 30-kDa membrane cutoff. Purification to homogeneity was achieved by fast-performance liquid chromatography using a UNO-Q12 anion exchange column equilibrated with 100 mM HEPES buffer (pH 7.5). The proteins were eluted at a flow rate of 3 ml/min by using a linear NaCl gradient ranging from 0 to 1 M in the same HEPES buffer. Pooled fractions displaying L-AI activity were desalted and concentrated.

Protein quantification and electrophoresis. Protein concentrations were determined using Bradford's method with bovine serum albumin as the standard (3). The purified enzyme samples were allowed to migrate in 12% sodium dodecyl sulfate-polyacrylamide gel electrophoresis (SDS-PAGE) gels according to the method of Laemmli (16). Protein bands were visualized by Coomassie brilliant blue R-250 (Bio-Rad) staining.

Flame atomic absorption spectrometry analysis. For sample preparation, each mineralized sample was employed at a final concentration of 10 mg/ml. A Perkin-Elmer Analyst 200 atomic absorption spectrophotometer (Norwalk, CT), equipped with a deuterium lamp background correction system, was used for metal binding quantification. Manganese hollow cathode lamps (wavelength, 279.5 nm; slit, 0.2 nm; Perkin-Elmer) were used as the primary radiation source. Analytical measurements were based on the average absorbance under the conditions recommended by the manufacturer.

Protein identification. Extracted wild-type and mutant proteins were separated by SDS-PAGE. After staining with Coomassie blue Biosafe (Bio-Rad), bands corresponding to the expected molecular masses were excised from the gel and washed in acetonitrile–50 mM ammonium hydrogen carbonate (vol/vol). Thereafter, samples were stirred for 15 min and vacuum dried for 30 min, and 0.5 mg of trypsin (Promega) in 25 ml of ammonium hydrogen carbonate (50 mM) was added. Samples were digested for 16 h at 37°C. For matrix-assisted laser desorption ionization–time of flight (MALDI-TOF) analyses, 2 μl of trifluoroacetic acid (5%) was added to stop the trypsinolysis reaction. Peptide mixtures were analyzed using a cyano-4-hydroxycinamic matrix prepared at 5 mg/ml in 50% acetonitrile containing 0.1% trifluoroacetic acid. The trypsin autolytic peptides (842.5 and 2,211.1 Da) were used as internal calibrators. Peptides with masses in the range of 700 to 4,000 Da were selected.

Peptides were analyzed using a Voyager DE STR MALDI-TOF mass spectrometer (Applied Biosystems). Recorded tandem mass spectrometry spectra were compared to theoretical fragmentations of a trypsinolyzed US100 AraA protein (accession number CAI29261) via the Sequest algorithm incorporated in the BioWorks software (version 2; Thermo Finnigan).

Enzyme assays and kinetic parameter determination. L-Arabinose isomerase activity was measured by determining the amount of L-ribulose or L-fuculose formed. Under standard conditions, the reaction mixture contained 0.2 mM $CoCl_2$, 1 mM $MnSO_4$, 50 μl of the enzyme preparation at a suitable dilution, 5 mM L-arabinose (or L-fucose), and 100 mM HEPES buffer (pH 7.5) in a final volume of 1 ml. The reaction mixture was incubated at 80°C for 1 and 10 min for

L-arabinose and L-fucose, respectively, followed by cooling of the samples on ice to stop the reaction. The amount of L-ribulose or L-fuculose generated was determined by the cysteine carbazole sulfuric acid method, and the absorbance at 560 nm was measured (6).

For determination of the kinetic parameters, assays were carried out under standard conditions by using 1 to 800 mM substrate (L-arabinose or L-fucose).

One unit of L-arabinose isomerase activity was defined as the amount of enzyme catalyzing the formation of 1 μmol of ketosugar per min under the above-specified conditions.

Amino acid sequence analysis and homology modeling. Sequence analysis and multiple alignments were done using the programs BLAST and CLUSTALW (1, 34). The secondary structure of the protein was predicted using the DSSP program (11), and rendering of the alignment including the superimposition of secondary structures was performed with the program ESPript (8). The 3D homology model of US100 L-AI was generated using the Geno3D server (5), and the superposition of 3D structures was performed with the "rigid" option in the graphics software TURBO-FRODO (29). Images were generated using TURBO-FRODO, and the surface rendering was done with UCSF Chimera (http://www.cgl.ucsf.edu/chimera).

RESULTS AND DISCUSSION

Structural analysis of the US100 L-AI active site and comparison with that of *E. coli* L-FI. Until now, no detailed analysis of the isomerization mechanism and the catalytic residues implicated in the reaction in the L-AI family has been reported. This prompted us to undertake the identification of crucial catalytic residues by using all available data. The 3D crystal structure of the L-fucose isomerase from *E. coli*, also known as D-arabinose isomerase (Protein Data Bank identification, 1FUI), was solved previously (31). In that previous work, the catalytic residues were reported to be E337, D361, and H528 and to interact with a manganese ion (Mn^{2+}). Furthermore, the 3D structure of the hexameric *E. coli* L-AI (Protein Data Bank identification, 2AJT) which displays 60% sequence identity to the US100 L-AI was solved previously (23). The authors of the study reported that this crystal structure was manganese depleted. More recently, coordinates for the 3D structure of the same *E. coli* L-AI but this time with a bound Mn^{2+} ion were deposited in the Protein Data Bank (identification, 2HXG; M. R. Chance, W. Zhu, and B. A. Manjasetty, unpublished results). After the superimposition of the two *E. coli* L-AI structures, 2AJT (Mn^{2+} depleted) and 2HXG (containing Mn^{2+}), an inspection of the active-site region showed that residues H350 and H450 displayed similar orientations in the two structures whereas the orientations of E306 and E333 differed slightly due to the presence in 2HXG of Mn^{2+} instead of a putative water molecule as in the published structure of 2AJT (23).

Taking advantage of this newly solved structure and using molecular-modeling techniques, we have constructed a 3D model of US100 L-AI. The generated model has a root mean square deviation of 1.5 Å from that of *E. coli* L-AI (2HXG) when C-α atoms are superimposed. As shown in Fig. 1, the presumed essential catalytic residues of *E. coli* L-AI as well as those of US100 L-AI (described hereafter) were perfectly superimposed onto those of *E. coli* L-FI. By analogy with *E. coli* L-FI catalytic residues E337, D361, and H528, residues E306, E331, and H447 from the US100 L-AI enzyme were deduced to be the essential catalytic amino acids. In order to confirm this observation, site-directed mutagenesis was employed to replace these amino acids with alanine.

Monitoring of the US100 L-AI activity by using crude protein extracts demonstrated that whereas an appreciable activity of the wild-type US100 L-AI of 46 U/mg was detected, no measurable activity of the E306A, E331A, and H447A mutants was detected. Note that the activity assays were performed at the optimal temperature (80°C) as well as at 50°C, at which the enzyme is completely thermostable.

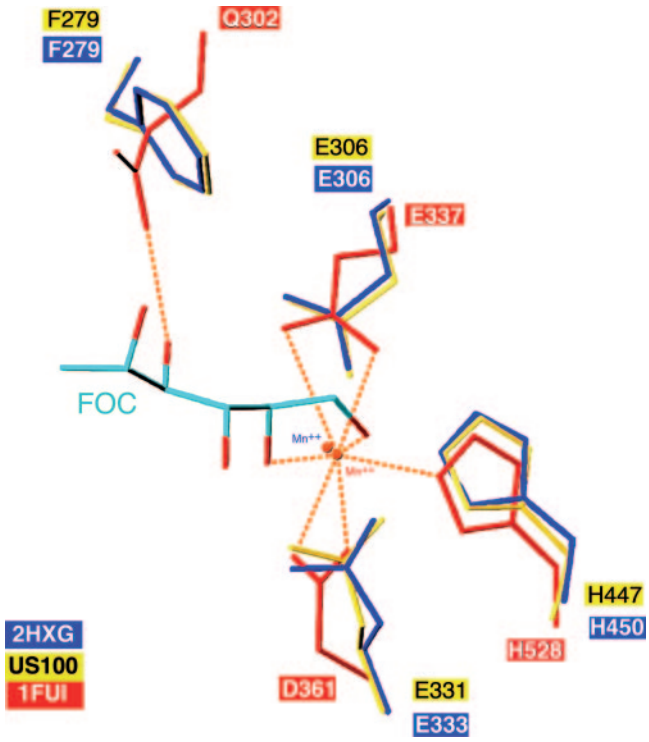

FIG. 1. Superposition of the three catalytic residues from *E. coli* L-AI (Protein Data Bank identification, 2HXG; in dark blue) onto *E. coli* L-FI (Protein Data Bank identification, 1FUI; in red) and the US100 L-AI model (yellow). L-Fucitol (FOC), shown in light blue, interacts with the Mn^{2+} ion (brown spheres). Note also the location of F279 in the US100 L-AI model and its corresponding residue, Q302, in the three-dimensional structure of *E. coli* L-FI.

With the aim of proving that these mutated proteins were inactive but efficiently expressed, the crude protein was analyzed by SDS-PAGE. As shown in Fig. 2A, all mutant enzymes were successfully overexpressed, with bands displaying a molecular mass of 56 kDa as expected for a monomer of US100 L-AI (28). Furthermore, an analysis of these bands by mass spectrometry (results not shown) confirmed the desired mutations.

One may thus conclude that the loss of activity of the reported mutants stems from the role of the corresponding mutated residues as catalytic residues in the isomerization reaction.

Other crucial catalytic residues of US100 L-AI. On the basis of the US100 L-AI model, an analysis of the active-site region indicated additional amino acids which could be implicated in the catalytic mechanism. As illustrated in Fig. 3, H348, which is highly conserved among all reported L-AIs (Fig. 4), is located in a position where it can interact with the manganese ion and/or the substrate. These observations incited us to mutate H348 into an alanine. The expression of the US100 L-AI

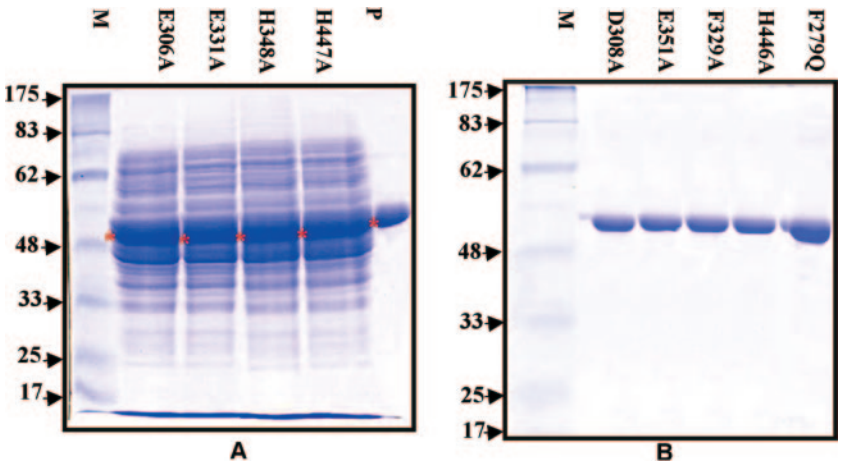

FIG. 2. SDS-PAGE analysis of the crude extract (A) and purified protein (B) derived from wild-type and mutant US100 L-AIs, with molecular masses in kilodaltons. (A) Lane M contains protein markers, and lanes E306A, E331A, H348A, and H447A show total cell extracts corresponding to US100 L-AI proteins with the indicated mutations. Lane P corresponds to purified wild-type US100 L-AI. Asterisks indicate bands which have been analyzed by mass spectrometry. (B) Lane M contains protein markers and lanes D308A, E351A, F329A, H446A, and F279Q correspond to the purified US100 L-AI proteins with the indicated mutations.

H348A mutant was confirmed by SDS-PAGE (Fig. 2A) and MALDI-TOF (results not shown). Despite its efficient expression, the US100 L-AI H348A mutant was effectively inactive, demonstrating the crucial role of this residue in the isomerization reaction.

An investigation of amino acids neighboring the catalytic residues in the 3D homology model of US100 L-AI showed that E331, H348, and H447 interact with H446, E351, F329, and D308 and are in a position suitable for binding to the divalent ion and/or the substrate (Fig. 3). In addition, the alignment of the majority of L-AI sequences showed that not only the essential catalytic residues E306, E331, H348, and H447, but also

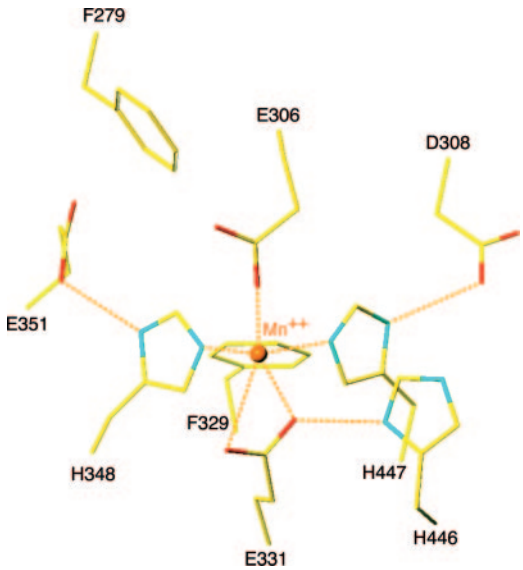

FIG. 3. Active-site region of the US100 L-AI model showing the catalytic residues E306, E331, and H447 and other crucial residues, such as H348 bound to a Mn^{2+} ion surrounded by residues E351, D308, and H446. F329 interacts with both H348 and H447 and seems to favor their interaction with the Mn^{2+} ion (brown sphere).

D308, E351, F329, and H446, are highly conserved (Fig. 4). The role of these amino acids was studied by site-directed mutagenesis of the US100 L-AI enzyme. Hence, mutant enzymes carrying the D308A, E351A, F329A, and H446A mutations were expressed and purified (Fig. 2B). Monitoring of the L-AI activities of purified D308A, E351A, F329A, and H446A mutants showed specific activities of 21, 27, 53, and 79 U/mg, respectively, compared to 184 U/mg for the purified wild-type enzyme. As illustrated in Table 2, in addition to their decrease in activity, these mutants showed a substantial decrease in turnover (k_{cat}) compared to the wild-type enzyme. Moreover, they displayed a limited alteration of the corresponding K_m values, thus suggesting that these residues are implicated in catalysis rather than the binding of the substrate. This is in agreement with the US100 L-AI model, which shows that these amino acids a priori are not in a position where they interact with the substrate directly, but indirectly via the essential catalytic residues. The role of these second-shell amino acids appears to be the stabilization of appropriate conformations of the former residues for interaction with the substrate. Analyses of the altered activities and of the catalytic properties showed that the D308A and E351A mutations provoked a greater decrease in the activities and k_{cat} values, with values for the corresponding mutants of 162.1 ± 0.08 and 174.3 ± 0.01 min^{-1}, respectively, than the mutation of H446 and F329, with k_{cat} values for the corresponding mutants of 857.7 ± 0.12 and 639.2 ± 0.06 min^{-1}, respectively (Table 2).

This decrease in activity and enzyme turnover can be explained by the direct interaction of E351 and D308 with H348 and H447, respectively, resulting in the stabilization of these residues. As concerns F329, it appears to be in a position suitable for maintaining H447 and H348 in an orientation adequate for interaction with Mn^{2+} (Fig. 3). H446 may interact with E331 via a hydrogen bond, allowing the binding of E331 to the Mn^{2+} ion.

These results indicate that D308, E351, F329, and H446 are implicated in the isomerization reaction as they contrib-

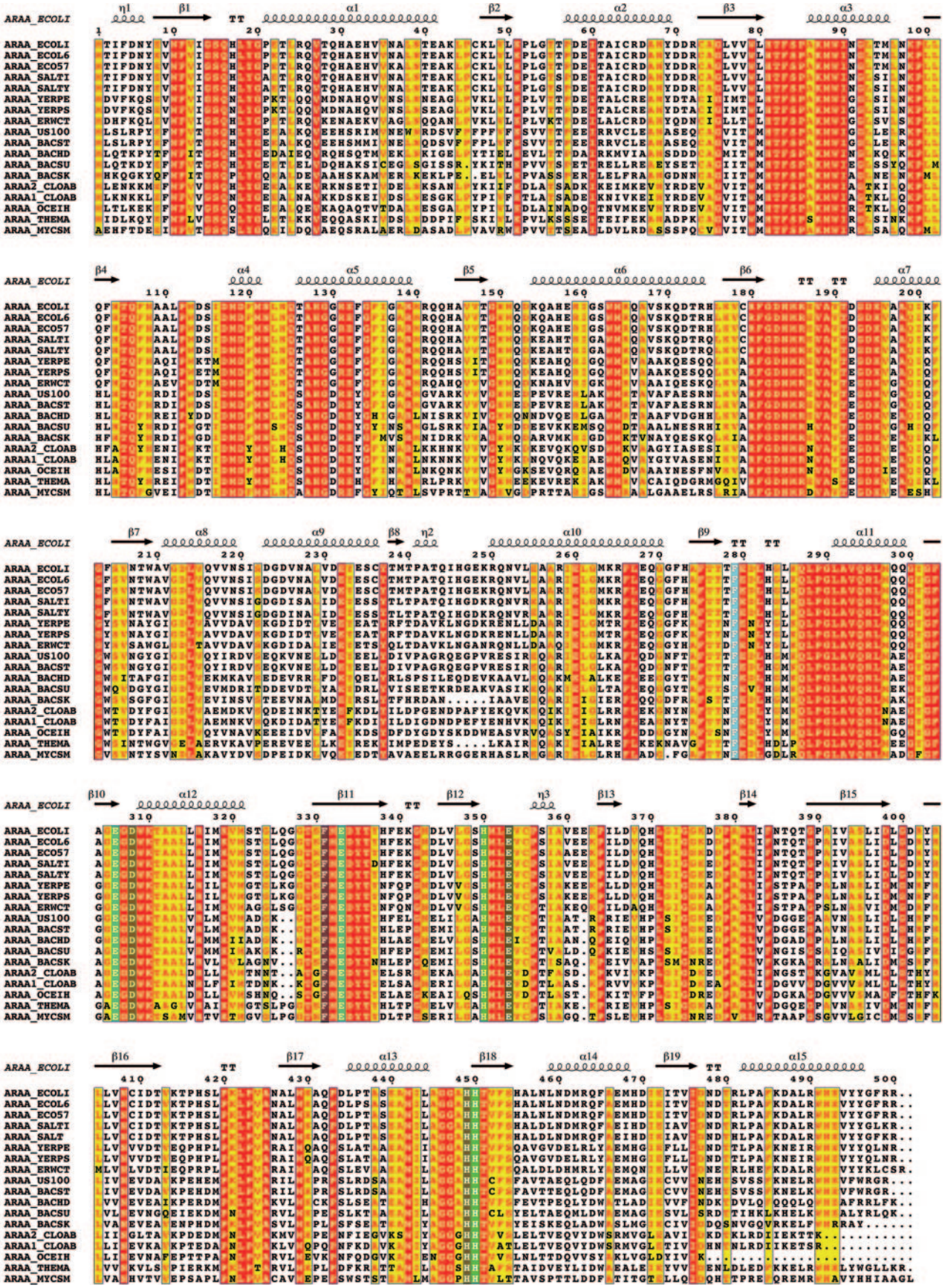

TABLE 2. Kinetic parameters determined for US100 L-AIs (wild type and mutants)[a]

Enzyme	K_m (mM)	k_{cat} (min^{-1})	k_{cat}/K_m (mM^{-1} min^{-1})	Activity loss (%)
WT	28.42 ± 0.12	2036.4 ± 0.07	71.65	0
D308A mutant	29.3 ± 0.31	162.1 ± 0.08	5.53	88
E351A mutant	30.1 ± 0.09	174.3 ± 0.01	5.79	85
F329A mutant	30.6 ± 0.15	639.2 ± 0.06	20.88	71
H446A mutant	30.4 ± 0.28	857.7 ± 0.12	28.21	57

[a] Assays were performed under standard conditions by using L-arabinose as the substrate. Results are mean values ± standard deviations from triplicate experiments. WT, wild-type US100 L-AI.

TABLE 3. Kinetic parameters determined for F279Q mutant[a]

Substrate and enzyme	K_m (mM)	k_{cat} (min^{-1})	k_{cat}/K_m (mM^{-1} min^{-1})
L-Arabinose			
F279Q mutant	79.7 ± 0.048	1893.1 ± 0.13	23.75
L-Fucose			
WT	ND	ND	ND
F279Q mutant	173.6 ± 0.042	946.7 ± 0.19	5.45

[a] Assays were performed under standard conditions. Results are mean values ± standard deviations from triplicate experiments. ND, not detected; WT, wild-type US100 L-AI.

ute to stabilizing H348, E331, E306, and H447, as illustrated in Fig. 3.

Evidence of the presence of manganese. The presence of manganese in the crystal structure of *E. coli* L-FI has been reported previously (31), and very recently the structure of *E. coli* L-AI with a bound manganese ion appeared in the Protein Data Bank (identification, 2HXG; Chance et al., unpublished results). In the case of US100 L-AI, the enzyme was purified in the absence of metallic ions and treated with 10 mM EDTA, followed by dialysis against 100 mM MOPS (morpholinopropanesulfonic acid; pH 7.5). As previously reported by Rhimi and Bejar, measurements of wild-type US100 L-AI activity before and after EDTA treatment showed no significant difference. This behavior is similar to that of *Bacillus halodurans*, *E. coli*, and *Lactobacillus gayonii* L-AIs but in contrast with that of all other reported L-AIs which require metal ions for their activity and thermal stability (18, 25, 26, 28).

In order to gain further insights on this issue, and more precisely on the presence of manganese ions in US100 L-AI, we analyzed the composition of the purified EDTA-treated US100 L-AI by flame atomic absorption spectrometry. The obtained results indicated the presence of manganese ions in the protein, evaluated at 3.6 ± 0.08 mol/mol of tetrameric enzyme and thus approximately one manganese ion per US100 L-AI monomer. This finding strongly suggests that manganese is closely bound to the enzyme even after EDTA treatment. Such a phenomenon has been reported previously for many proteases in which the calcium ion was intimately fixed to the enzyme (21, 27).

These results are in agreement with those from previous work indicating the implication of a divalent ion in the isomerization reaction which can proceed via two distinct pathways: hydride shift and *cis*-enediol. For xylose isomerases (EC 5.3.1.5), the conversion of xylose into xylulose is performed via a hydride shift mechanism using manganese ions as the cofactor (2, 7), whereas for triosephosphate isomerase (EC 5.3.1.1), the interconversion of dihydroxyacetone phosphate and glyceraldehyde 3-phosphate occurs via the *cis*-enediol pathway (22, 32, 33).

The analyses of the inactive US100 L-AI mutants (those with mutations E306A, E331A, and H447A) by using flame atomic absorption spectrometry showed that manganese was present at levels similar to that in the wild-type US100 L-AI. Moreover, the K_m corresponding to the D308A, H446A, E351A, and F329A mutants for Mn^{2+} was nearly the same as that of the wild type, 25.6 mM. Therefore, the activity loss seems directly correlated to the replacement of the amino acids rather than a loss or a weakening of the binding of manganese.

Influence of F279 on enzyme affinity. An inspection of the US100 L-AI model superimposed onto the structure of *E. coli* L-AI (2HXG) showed that F279 was located close to the active site (Fig. 1). In the 3D structure of *E. coli* L-FI, the corresponding residue, Q302, is in a favorable position to be involved in substrate recognition (Fig. 1). Furthermore, the alignment of several L-AI primary structures shows that this residue is highly conserved among all reported sequences (Fig. 4), thus reinforcing the hypothesis that this residue is putatively important. In order to confirm the importance of this residue, the US100 L-AI F279Q mutant was constructed and purified to homogeneity (Table 1; Fig. 2B).

As shown in Table 3, wild-type US100 L-AI is unable to convert L-fucose into L-fuculose whereas the F279Q mutant exhibited notable isomerase activity, evaluated as 18 U/mg, when using L-fucose as the substrate.

The kinetic parameters of the wild-type enzyme and the US100 L-AI F279Q mutant, when using L-arabinose as the

FIG. 4. Structure-based multiple sequence alignment of US100 L-AI with other L-AIs. Residues invariable among sequences are in white type on a red background, residues conserved within each group are displayed as red letters on a yellow background, and catalytic residues are shown in green. Residues which have a putative stabilizing role are displayed in brown. The residue mutated for affinity studies is in light blue. The secondary structure elements from the crystal structure of *E. coli* L-AI are indicated at the top of the alignment. ARAA-ECOLI, *E. coli* (PO8202) (Protein Data Bank identification, 2HXG); ARAA-ECOL6, *E. coli* (Q8LF89); ARAA-ECO57, *E. coli* (P58538); ARAA-SALTI, *Salmonella enterica* serovar Typhimurium (P58539); ARAA-SALTY, *S. enterica* serovar Typhimurium (P06189); ARAA-YERPE, *Yersinia pestis* (P58540); ARAA-YERPS, *Yersinia pseudotuberculosis* (Q66AF8); ARAA-YERPE, *Pectobacterium atrosepticum* (Q6D4W5); ARAA-US100, *Geobacillus stearothermophilus* US100 (CAI29261); ARAA-BACST, *Geobacillus stearothermophilus* (Q9S467); ARAA-BACHD, *Bacillus halodurans* (Q9KBQ2); ARAA-BACSU, *Bacillus subtilis* (P94523); ARAA-BACSK, *Bacillus clausii* KSM-K16 (Q5WL05); ARAA2-COLAB, *Clostridium acetobutylicum* (Q97JE4); ARAA1-COLAB, *Clostridium acetobutylicum* (Q97JE0); ARAA-OCEIH, *Oceanobacillus iheyensis* (Q8EMP4); ARAA-THEMA, *Thermotoga maritima* (Q9WYB3); ARAA-MYCSM, *Mycobacterium smegmatis* (Q9RAG2). The US100 AraA sequence is indicated by arrows on the left.

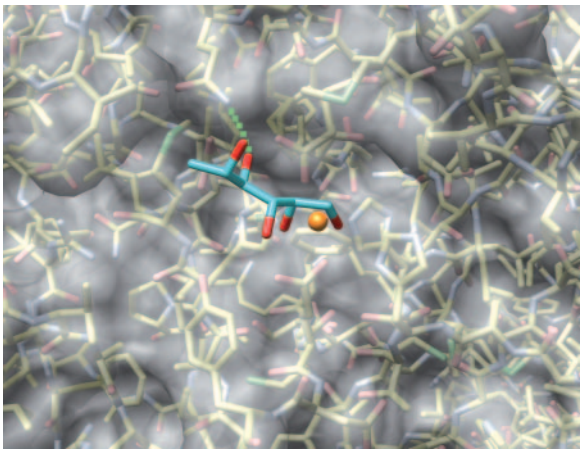

FIG. 5. Molecular surface representation of US100 L-AI, around the active center. The substrate L-fucitol has been modeled into the active site of US100 L-AI on the basis of the *E. coli* L-FI–L-fucitol complex structure. The Mn^{2+} ion located near the substrate in the active site is shown as a brown sphere. F279 has been replaced by Q279, and the putative interaction of this residue with L-fucitol (in blue) is presented.

substrate, showed a significant increase of the estimated K_m to 79.7 mM instead of 28.4 mM, with a concomitant decrease in the catalytic efficiency (k_{cat}/K_m) (Tables 2 and 3). Nevertheless, the mutant enzyme turnover was slightly decreased to 1,893.1 min^{-1} compared to 2,036.4 min^{-1} for wild-type US100 L-AI. These results suggest that the F279Q mutation is implicated in substrate recognition rather than catalysis. Moreover, the mutant corresponded to a K_m of 173.6 mM and a catalytic efficiency of 5.45 mM^{-1} min^{-1} with L-fucose (Table 3). These results are in accordance with F279 being in a suitable position to interact with the substrate, as seen in the 3D homology model of US100 L-AI (Fig. 5).

We therefore conclude that mutating F279 to Q279 shifts the affinity of US100 L-AI in favor of L-fucose and decreases the affinity for L-arabinose.

In this study, we have identified nine amino acids of the US100 L-AI that are highly conserved within reported sequences of L-AIs. Using molecular modeling and site-directed mutagenesis, we have demonstrated that these residues are intimately involved in substrate recognition and in the isomerization reaction. Wild-type US100 L-AI and selected mutants will be subjected to X-ray crystallography studies in order to contribute to the understanding of the details of the isomerization mechanism.

ACKNOWLEDGMENTS

This research was supported by the Tunisian government contract program CBS-LEMP (Centre de Biotechnologie de Sfax-Laboratoire d'Enzymes et Métabolites des Procaryotes) and by the French-Tunisian program CMCU (Comité Mixte de Coopération Universitaire, no. 04/0905).

We express our gratitude to Néji Gharsallah and Emmanuelle Maguin for their generous help and support.

REFERENCES

1. **Altschul, S. F., T. L. Madden, A. A. Schaffer, J. Zhang, Z. Zhang, W. Miller, and D. J. Lipman.** 1997. Gapped BLAST and PSI-BLAST: a new generation of protein database search programs. Nucleic Acids Res. **25:**3389–3402.
2. **Blow, D. M., C. A. Collyer, J. D. Goldberg, and O. S. Smart.** 1992. Structure and mechanism of D-xylose isomerase. Faraday Discuss., p. 67–73.
3. **Bradford, M. M.** 1976. A rapid and sensitive method for the quantification of microgram quantities of protein utilizing the principle of protein-dye binding. Anal. Biochem. **72:**248–254.
4. **Cheetam, P. S. J., and A. N. Woottom.** 1993. Bioconversion of D-galactose into D-tagatose. Enzyme Microb. Technol. **15:**105–108.
5. **Combet, C., M. Jambon, G. Deleage, and C. Geourjon.** 2002. Geno3D: automatic comparative molecular modelling of protein. Bioinformatics **18:** 213–214.
6. **Dische, Z., and E. Borenfreund.** 1951. A new spectrophotometric method for the detection and determination of keto sugars and trioses. J. Biol. Chem. **192:**583–587.
7. **Fenn, T. D., D. Ringe, and G. A. Petsko.** 2004. Xylose isomerase in substrate and inhibitor michaelis states: atomic resolution studies of a metal-mediated hydride shift. Biochemistry **43:**6464–6474.
8. **Gouet, P., X. Robert, and E. Courcelle.** 2003. ESPript/ENDscript: extracting and rendering sequence and 3D information from atomic structures of proteins. Nucleic Acids Res. **31:**3320–3323.
9. **Izumori, K., Y. Ueda, and K. Yamanaka.** 1978. Pentose metabolism in *Mycobacterium smegmatis*: comparison of L-arabinose isomerases induced by L-arabinose and D-galactose. J. Bacteriol. **133:**413–414.
10. **Jorgensen, F., O. C. Hansen, and P. Stougaard.** 2004. Enzymatic conversion of D-galactose to D-tagatose: heterologous expression and characterisation of a thermostable L-arabinose isomerase from *Thermoanaerobacter mathranii*. Appl. Microbiol. Biotechnol. **64:**816–822.
11. **Kabsch, W., and C. Sander.** 1983. Dictionary of protein secondary structure: pattern recognition of hydrogen-bonded and geometrical features. Biopolymers **22:**2577–2673.
12. **Kim, B. C., Y. H. Lee, H. S. Lee, D. W. Lee, E. A. Choe, and Y. R. Pyun.** 2002. Cloning, expression and characterization of L-arabinose isomerase from *Thermotoga neapolitana*: bioconversion of D-galactose to D-tagatose using the enzyme. FEMS Microbiol. Lett. **212:**121–126.
13. **Kim, H. J., J. H. Kim, H. J. Oh, and D. K. Oh.** 2006. Characterization of a mutated *Geobacillus stearothermophilus* L-arabinose isomerase that increases the production rate of D-tagatose. J. Appl. Microbiol. **101:**213–221.
14. **Kim, J. W., Y. W. Kim, H. J. Roh, H. Y. Kim, J. H. Cha, K. H. Park, and. C. S. Park.** 2003. Production of tagatose by a recombinant thermostable L-arabinose isomerase from *Thermus* sp. IM6501. Biotechnol. Lett. **25:**963–967.
15. **Kim, P., S. H. Yoon, M. J. Seo, D. K. Oh, and J. H. Choi.** 2001. Improvement of tagatose conversion rate by genetic evolution of thermostable galactose isomerase. Biotechnol. Appl. Biochem. **34:**99–102.
16. **Laemmli, U. K.** 1970. Cleavage of structural proteins during the assembly of the head of bacteriophage T4. Nature **227:**680–685.
17. **Lee, D., H. Jang, E. Choe, B. Kim, S. Lee, S. Kim, Y. Hong, and Y. Pyun.** 2004. Characterization of a thermostable L-arabinose (D-galactose) isomerase from the hyperthermophilic eubacterium *Thermotoga maritima*. Appl. Environ. Microbiol. **70:**1397–1404.
18. **Lee, D. W., E. A. Choe, S. B. Kim, S. H. Eom, Y. H. Hong, S. J. Lee, H. S. Lee, D. Y. Lee, and Y. R. Pyun.** 2005. Distinct metal dependence for catalytic and structural functions in the L-arabinose isomerases from the mesophilic *Bacillus halodurans* and the thermophilic *Geobacillus stearothermophilus*. Arch. Biochem. Biophys. **434:**333–343.
19. **Lee, S. J., D. W. Lee, E. A. Choe, Y. H. Hong, S. B. Kim, B. C. Kim, and Y. R. Pyun.** 2005. Characterization of a thermoacidophilic L-arabinose isomerase from *Alicyclobacillus acidocaldarius*: role of Lys-269 in pH optimum. Appl. Environ. Microbiol. **71:**7888–7896.
20. **Levin, G. V., L. R. Zehner, J. P. Saunders, and J. R. Beadle.** 1995. Sugar substitutes: their energy values, bulk characteristics, and potential health benefits. Am. J. Clin. Nutr. **62:**1161S–1168S.
21. **Lin, S. J., E. Yoshimura, H. Sakai, T. Wakagi, and H. Matsuzawa.** 1999. Weakly bound calcium ions involved in the thermostability of aqualysin I, a heat-stable subtilisin-type protease of *Thermus aquaticus* YT-1. Biochim. Biophys. Acta **1433:**132–138.
22. **Mande, S. C., V. Mainfroid, K. H. Kalk, K. Goraj, J. A. Martial, and W. G. Hol.** 1994. Crystal structure of recombinant human triosephosphate isomerase at 2.8 A resolution. Triosephosphate isomerase-related human genetic disorders and comparison with the trypanosomal enzyme. Protein Sci. **3:**810–821.
23. **Manjasetty, B. A., and M. R. Chance.** 2006. Crystal structure of *Escherichia coli* L-arabinose isomerase (ECAI), the putative target of biological tagatose production. J. Mol. Biol. **360:**297–309.
24. **Mazur, A. W.** May 1989. Functional sugar substitutes with reduced calories. European patent 341062.
25. **Nakamatu, T., and K. Yamanaka.** 1969. Crystallization and properties of L-arabinose isomerase from *Lactobacillus gayonii*. Biochim. Biophys. Acta **178:**156–165.
26. **Patrick, J. W., and N. Lee.** 1968. Purification and properties of an L-arabinose isomerase from *Escherichia coli*. J. Biol. Chem. **243:**4312–4318.
27. **Ravaud, S., P. Gouet, R. Haser, and N. Aghajari.** 2003. Probing the role of divalent metal ions in a bacterial psychrophilic metalloprotease: binding

studies of an enzyme in the crystalline state by X-ray crystallography. J. Bacteriol. **185:**4195–4203.
28. **Rhimi, M., and S. Bejar.** 2006. Cloning, purification and biochemical characterization of metallic-ions independent and thermoactive L-arabinose isomerase from the *Bacillus stearothermophilus* US100 strain. Biochim. Biophys. Acta **1760:**191–199.
29. **Roussel, A., and C. Cambillau.** 1992. Architecture et fonction des macromolecules biologiques. Biographics, Marseille, France.
30. **Sambrook, J., E. F. Fritsh, and T. Maniatis.** 1989. Molecular cloning: a laboratory manual, 2nd ed. Cold Spring Harbor Laboratory Press. Cold Spring Harbor, NY.
31. **Seemann, J. E., and G. E. Schulz.** 1997. Structure and mechanism of L-fucose isomerase from *Escherichia coli*. J. Mol. Biol. **273:**256–268.
32. **Straus, D., R. Raines, E. Kawashima, J. R. Knowles, and W. Gilbert.** 1985. Active site of triosephosphate isomerase: in vitro mutagenesis and characterization of an altered enzyme. Proc. Natl. Acad. Sci. USA **82:**2272–2276.
33. **Swan, M. K., J. T. Solomons, C. C. Beeson, T. Hansen, P. Schonheit, and C. Davies.** 2003. Structural evidence for a hydride transfer mechanism of catalysis in phosphoglucose isomerase from *Pyrococcus furiosus*. J. Biol. Chem. **278:**47261–47268.
34. **Thompson, J. D., D. G. Higgins, and T. J. Gibson.** 1994. CLUSTAL W: improving the sensitivity of progressive multiple sequence alignment through sequence weighting, position-specific gap penalties and weight matrix choice. Nucleic Acids Res. **22:**4673–4680.
35. **Yamanaka, K.** 1975. L-Arabinose isomerase from *Lactobacillus gayonii*. Methods Enzymol. **41:**458–461.
36. **Zehner, L. R., G. V. Levin, J. P. Saunders, and J. R. Beadle.** October 1994. D-Tagatose as anti-hyperglycemic agent. U.S. patent 5,356,879.